Genetically encoded fluorescent probe to visualize intracellular phosphatidylinositol 3,5-bisphosphate localization and dynamics

Xinran Li[a], Xiang Wang[a], Xiaoli Zhang[a], Mingkun Zhao[a], Wai Lok Tsang[a], Yanling Zhang[b,c], Richard Gar Wai Yau[b,c], Lois S. Weisman[b,c], and Haoxing Xu[a,1]

[a]Department of Molecular, Cellular, and Developmental Biology, University of Michigan, Ann Arbor, MI 48109; and [b]Department of Cell and Developmental Biology and [c]Life Sciences Institute, University of Michigan, Ann Arbor, MI 48109-2216

Edited by Tamas Balla, National Institutes of Health, Bethesda, MD, and accepted by the Editorial Board November 15, 2013 (received for review June 21, 2013)

Phosphatidylinositol 3,5-bisphosphate [PI(3,5)P_2] is a low-abundance phosphoinositide presumed to be localized to endosomes and lysosomes, where it recruits cytoplasmic peripheral proteins and regulates endolysosome-localized membrane channel activity. Cells lacking PI(3,5)P_2 exhibit lysosomal trafficking defects, and human mutations in the PI(3,5)P_2-metabolizing enzymes cause lysosome-related diseases. The spatial and temporal dynamics of PI(3,5)P_2, however, remain unclear due to the lack of a reliable detection method. Of the seven known phosphoinositides, only PI(3,5)P_2 binds, in the low nanomolar range, to a cytoplasmic phosphoinositide-interacting domain (ML1N) to activate late endosome and lysosome (LEL)-localized transient receptor potential Mucolipin 1 (TRPML1) channels. Here, we report the generation and characterization of a PI(3,5)P_2-specific probe, generated by the fusion of fluorescence tags to the tandem repeats of ML1N. The probe was mainly localized to the membranes of Lamp1-positive compartments, and the localization pattern was dynamically altered by either mutations in the probe, or by genetically or pharmacologically manipulating the cellular levels of PI(3,5)P_2. Through the use of time-lapse live-cell imaging, we found that the localization of the PI(3,5)P_2 probe was regulated by serum withdrawal/addition, undergoing rapid changes immediately before membrane fusion of two LELs. Our development of a PI(3,5)P_2-specific probe may facilitate studies of both intracellular signal transduction and membrane trafficking in the endosomes and lysosomes.

TRP channel | PIKfyve | vesicle fusion

Phosphorylated phosphoinositide lipids are produced on the cytosolic side of cellular lipid bilayer membranes (1, 2). There are seven different known phosphoinositides lipids, which localize to distinct membrane subdomains to regulate organelle-specific membrane signaling pathways and membrane-trafficking events (1, 2). One such phosphoinositide lipid is phosphatidylinositol 4,5-bisphosphate [PI(4,5)P_2], which is predominantly localized to the plasma membrane (PM). PI(4,5)P_2 serves as a permissive cofactor that is required for the activity of PM channels/transporters, as a precursor for the generation of second messengers, and as a PM recruiter for cytosolic peripheral proteins (3, 4). Likewise, PI(3,4)P_2 and PI(3,4,5)P_3 are transiently produced at the PM to regulate various signaling effectors, such as v-akt-murine thymoma viral oncogene homolog 1 (Akt) (1, 5). Conversely, PI(3)P is primarily found on early endosomes, phagosomes, and autophagosomes to regulate the maturation of these compartments (5, 6).

Unlike the aforementioned phosphoinositides, the subcellular localization and functions of PI(3,5)P_2 are poorly understood. PI(3,5)P_2 is proposed to be mainly localized to late endosomes and lysosomes (LELs) (7), and also to early endosomes (8), based on the location of its synthesizing enzyme complex, which in mammalian cells consists of the phosphoinositide kinase, FYVE finger-containing (PIKfyve) the phosphatase FIG4 homolog, SAC1 lipid phosphatase domain-containing (Fig4), and the scaffolding protein VAC 14 homolog (Vac14) (9–12). Genetic disruption of any of these components in mice results in a decrease in the intracellular PI(3,5)P_2 level, lysosomal trafficking defects at the cellular level, and embryonic/neonatal lethality at the animal level (9–12). Consistent with the LEL localization of PI(3,5)P_2, we recently reported that PI(3,5)P_2 is an endogenous agonist for mucolipin TRP (TRPML) and two-pore TPC channels, which are LEL-localized membrane channel proteins (13, 14). Despite its genetic importance, the localization and dynamics of PI(3,5)P_2 remain to be established at the single-cell level, largely due to the lack of a direct method to visualize this low-abundance phosphoinositide.

The recent development of specific fluorescent probes has greatly enhanced our understanding of phosphoinositide signaling (2, 15). These probes include those for PI(3)P, PI(4)P, PI(3,4)P_2, PI(4,5)P_2, and PI(3,4,5,)P_3, which are generated by fusing fluorescent tags with the phosphoinositide-interacting domains of their effector proteins. For example, GFP or mCherry proteins are fused directly with the FAPP1-PH domain [for PI(4)P], the phospholipase C $(PLC)_\delta$-PH domain [for PI(4,5)P_2], the AKT-PH domain [for both PI(3,4)P_2 and PI(3,4,5)P_3], and the hepatocyte growth factor-regulated tyrosine kinase substrate (Hrs)-FYVE and early endosome antigen 1 (EEA1)-FYVE domains [for PI(3)P] (15, 16). However, an effective, high-affinity PI(3,5)P_2 probe is still lacking, possibly due to two barriers. First, most peripheral phosphoinositide-binding proteins exhibit low

Significance

Phosphatidylinositol polyphosphates (PIPs) are transiently generated at specific membrane subdomains. Changes of PIP levels regulate the trafficking of vesicles and the activity of membrane transport proteins. To directly visualize the intracellular dynamics of phosphatidylinositol 3,5-bisphosphate [PI(3,5)P_2], a key phosphoinositide in the endosome and lysosome, we have engineered a PI(3,5)P_2 probe by fusing fluorescent proteins directly to the lipid-binding domain of TRPML1, a lysosomal ion channel that is potently and specifically activated by PI(3,5)P_2. This PI(3,5)P_2 probe binds to PI(3,5)P_2 with biochemical specificity in vitro and responds quickly to changes in the intracellular PI(3,5)P_2 level in living cells. With this biosensor, rapid changes of PI(3,5)P_2 on single vesicle membranes are captured prior to membrane fusion of two vesicles.

Author contributions: X.L., X.W., and H.X. designed research; X.L., X.W., X.Z., M.Z., W.L.T., Y.Z., and R.G.W.Y. performed research; X.L. contributed new reagents/analytic tools; X.L., X.Z., Y.Z., R.G.W.Y., and L.S.W. analyzed data; and X.L. and H.X. wrote the paper.

The authors declare no conflict of interest.

This article is a PNAS Direct Submission. T.B. is a guest editor invited by the Editorial Board.

[1]To whom correspondence should be addressed. E-mail: haoxingx@umich.edu.

This article contains supporting information online at www.pnas.org/lookup/suppl/doi:10.1073/pnas.1311864110/-/DCSupplemental.

affinity binding and often require the simultaneous binding of additional factors to increase the affinity and specificity (2, 17). PI(3,5)P_2 is a poorly characterized phosphoinositide with very few known effectors, most of which exhibit relatively low affinities (18, 19). Second, intracellular PI(3,5)P_2 levels are reportedly low [around 1/10th of that of PI(3)P and less than 1/100th of that of PI(4,5)P_2] (2, 10, 12).

Thus, it has proven difficult to develop an effective PI(3,5)P_2 probe for in situ use by using the phosphoinositide-binding domains of peripheral proteins (18). We recently reported that TRPML1, a LEL-localized membrane channel protein, is potently activated by PI(3,5)P_2 in the low nanomolar range. We further showed that PI(3,5)P_2 binds to the cytosolic N-terminal polybasic domain of TRPML1 (ML1N). This specific activation/binding is abolished by mutations of basic residues within the polybasic domain (20). In this study, we report the development of a genetically encoded PI(3,5)P_2 fluorescent probe based on ML1N.

Results

A Fluorescent PI(3,5)P_2 Probe Based on the Phosphoinositide-Interacting Domain of TRPML1 Exhibits Membrane Localization That Is Dependent on PI(3,5)P_2. We previously showed that PI(3,5)P_2 activates TRPML1 with striking specificity and a low nanomolar EC_{50}, with no other phosphoinositides exhibiting any activation effect (20). Moreover, in vitro binding assays demonstrated that the glutathione S-transferase (GST) fusion protein of the cytosolic N-terminal segment (ML1N; residues 1–68) can bind directly to PI(3,5)P_2 (20). We reasoned that fusion of fluorescence tags with ML1N would serve as a high-affinity PI(3,5)P_2 sensor. To potentially increase the affinity and specificity (15), a tandem repeat of ML1N (ML1N*2) was fused with an N-terminal GFP or mCherry tag (Fig. S1). Indeed, the purified GST fusion proteins of GFP-ML1N*2 (GST-GFP-ML1N*2) exhibited a much higher specificity toward PI(3,5)P_2 in in vitro protein–lipid binding assays than the single-copy GST-ML1N used in our previous study (20). In the liposome binding assay, which would best mimic the "vesicular membrane environment" in living cells, the GST-GFP-ML1N*2 proteins specifically recognized PI(3,5)P_2 with a K_d of 5.6 μM (Fig. S2), but not any other phosphoinositides tested except for weak binding to PI(5)P (Fig. 1*A*). In the PIP strip and PIP-beads binding assays, the tandem fusion proteins also exhibited a weak binding to PI(4,5)P_2, PI(3,4,5)P_3, and PI(3)P (Figs. S3 and S4). Nevertheless, much stronger binding was seen for PI(3,5)P_2, with no obvious binding to most other phospholipids (Figs. S3 and S4). Collectively, these results indicated that the tandem probe manifests a high in vitro specificity for PI(3,5)P_2 over other phosphoinositides.

To determine the intracellular localization of the probe, COS1 cells were cotransfected with either GFP- or mCherry-tagged ML1N*1 or ML1N*2 probes. The ML1N*1 probe was mainly localized to the cytosol, with limited localization on lysosome-associated membrane protein 1 (Lamp1)-positive vesicular membranes (Fig. S5). In contrast, significant amounts of GFP-ML1N*2 or mCherry-ML1N*2 were localized to the membranes of Lamp1-positive vesicles in COS1 cells (Fig. 1*B* and Fig. S6).

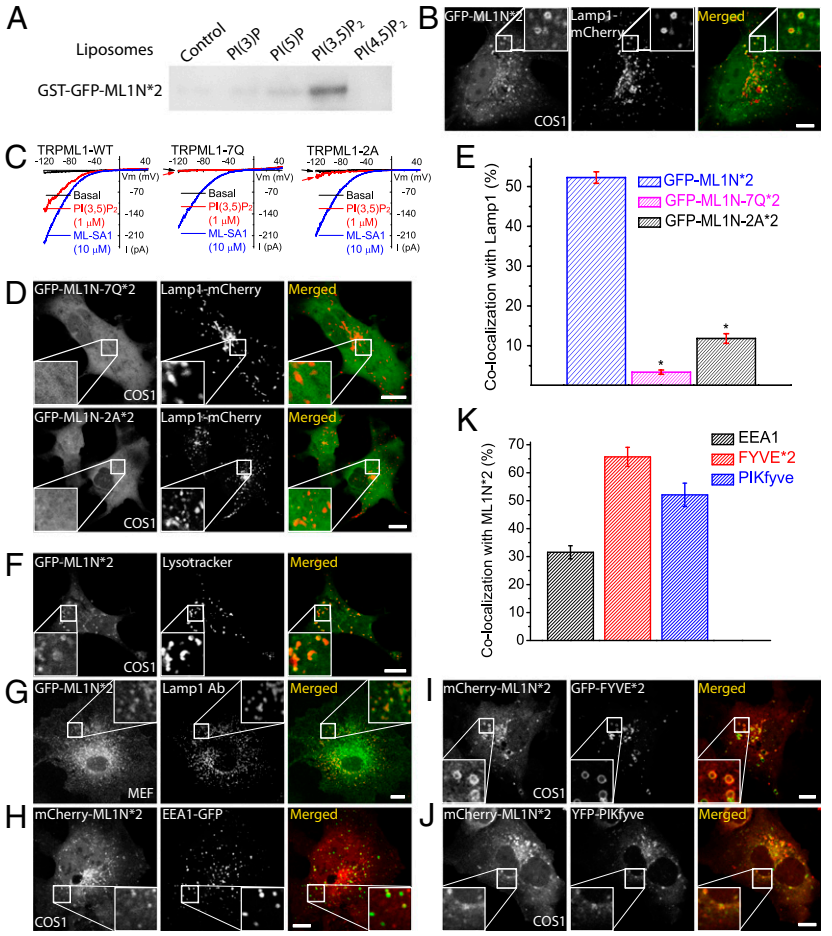

Fig. 1. Colocalization of the ML1N-based PI(3,5)P_2 probe with endolysosomal markers. (*A*) Purified GST-GFP-ML1N*2 proteins bound strongly to PI(3,5)P_2-containing liposomes, but not to liposomes containing PI(3)P, PI(5)P, or PI(4,5)P_2. Liposomes, diluted to a final concentration of 20 μM total lipids with 1 μM tested phosphoinositide, were incubated with purified GST-fusion proteins for 20 min, centrifuged, and visualized by Western blot with GST antibodies. (*B*) GFP-ML1N*2 exhibited a vesicular location and significant colocalization with Lamp1-mCherry. Confocal images were taken 24 h posttransfection in COS1 cells that were cotransfected with Lamp1-mCherry and GFP-ML1N*2. (*C*) Charge-neutralizing mutations in the phosphoinositide-interacting domain ($R^{42}Q/R^{43}Q/R^{44}Q/K^{55}Q/R^{57}Q/R^{61}Q/K^{62}Q$, abbreviated as 7Q; $R^{61}A/K^{62}A$, abbreviated as 2A; also see ref. 21) selectively impaired or abolished the activation of TRPML1 by PI(3,5)P_2 (1 μM) in the whole-endolysosome configuration; enlarged endolysosomes were isolated from COS1 cells transfected with various TRPML1 constructs. In contrast, ML-SA1 readily activated wild-type (WT) TRPML1, TRPML1-7Q, and TRPML1-2A in the same endolysosomes. (*D*) The localization of the ML1N*2 probe to vacuolar membranes was dependent on the basic residues in its phosphoinositide-interacting domain. Both ML1N-7Q*2 and ML1N-2A*2 displayed a diffuse, cytosolic localization pattern. (*E*) Quantification of the colocalization index between ML1N*2 and Lamp1 (see *SI Materials and Methods* for the algorithm that was used to analyze the colocalization). (*F*) Colocalization of GFP-ML1N*2 with LysoTracker (red) in COS1 cells. (*G*) Colocalization of GFP-ML1N*2 with endogenous Lamp1 (recognized by a Lamp1 antibody) in MEF cells. (*H–K*) Colocalization analyses between ML1N*2 and other fluorescently tagged endolysosomal proteins/markers in COS1 or MEF cells that were transfected with the indicated constructs for 24 h. (*H*) Colocalization of mCherry-ML1N*2 with the early endosomal marker GFP-EEA1. (*I*) Colocalization of ML1N*2 with the PI(3)P probe GFP-Hrs-FYVE*2. (*J*) Colocalization of ML1N*2 with YFP-PIKfyve. (*K*) Quantitative analyses revealed that ML1N*2 exhibited various degrees of colocalization with YFP-PIKfyve, GFP-FYVE*2, and GFP-EEA1. Error bars represent SEM; numbers of data points are given in the text. The asterisk indicates $P < 10^{-5}$. (Scale bar: 10 μm.)

Previous studies of other phosphoinositide probes, such as the PLC_{δ}-PH-GFP domain for $PI(4,5)P_2$ or the Hrs-FYVE domain for PI(3)P, have shown that mutations of key phosphoinositide-binding residues are sufficient to decrease, or even block, the localization of the probe to specific membranes (15, 16). We thus also investigated whether mutational analysis would decrease or abolish the vacuolar localization of the ML1N*2 probe. Seven positively charged amino acid residues in the phosphoinositide-interacting domain (Fig. S1*B*) have been shown to be crucial for $PI(3,5)P_2$ activation/binding (20, 21). Further analyses demonstrated that two of these residues, Arg-61 and Lys-62, mediated the majority of the activation effect in the whole-endolysosome recording (Fig. 1*C*) or whole-cell recording of surface-expressed TRPML1 (21). We mutated all seven positively charged residues to Gln (abbreviated as 7Q) or specifically mutated the Arg-61 and Lys-62 residues to Ala (abbreviated as 2A) in the ML1N*2 background. Interestingly, the ML1N-7Q*2 probe, which exhibited a loss of its binding capability to $PI(3,5)P_2$ in the protein–lipid interaction assays (20), showed a diffuse cytosolic pattern (Fig. 1*D*, *Upper*). Likewise, the ML1N-2A*2 mutant probe also exhibited a similar cytosolic localization, although very weak localization to Lamp1-positive vesicles was also observed (Fig. 1*D*, *Lower*), possibly due to an incomplete loss of $PI(3,5)P_2$ affinity compared with the ML1N-7Q*2 probe (Fig. 1*C*). In quantitative analyses, whereas ML1N-7Q*2 was completely mislocalized (3.4 ± 0.5%, $n = 18$), ML1N-2A*2 still exhibited a very low level (11.8 ± 1.2%, $n = 24$) of colocalization with Lamp1 (Fig. 1*E*). These results suggest that the level of colocalization correlates with the $PI(3,5)P_2$ binding affinity of ML1N*2.

The ML1N*2 $PI(3,5)P_2$ Probe Is Localized to Endolysosomal Compartments in Mammalian Cells. To further define the locations of the probe, cells were cotransfected or stained with various organellar markers of the endocytic pathway (Fig. 1 *F*–*K*). In agreement with the subcellular locations of the $PI(3,5)P_2$-synthesizing enzyme complex (8), the ML1N*2 probe colocalized highly with the LEL marker Lamp1 (Fig. 1 *B* and *G* and Fig. S6*A*). Nevertheless, most ML1N*2-expressing cells also exhibited additional cytosolic, nonvesicular localization (Fig. 1*B* and Fig. S6*A*), which could be attributed to a combination of a high level of probe expression (15) and a low level of basal $PI(3,5)P_2$. To account for this observation, positive "colocalization" was set arbitrarily as the number of pixels positive for the endocytic markers when the fluorescent intensity of the probe (membrane-bound fluorescence intensity) was more than 150% of the cytosolic, "background" intensity (see *SI Materials and Methods* for a detailed description of the colocalization analysis). With this algorithm, the colocalization index in the control experiments was >90% for Lamp1-mCherry and Lamp1-EGFP, but <1% for mCherry and Lamp1-EGFP, indicative of the reliability of the analysis (Fig. S7). In COS1 cells, about one-half of the Lamp1 fluorescence signal (52.3 ± 1.4%, $n = 45$ cells; Fig. 1*E*) colocalized with the ML1N*2 probe (Fig. 1*B*). A high degree of colocalization between ML1N*2 and Lamp1 was also observed in other cell types including mouse embryonic fibroblast (MEF), Chinese hamster ovary (CHO), and human embryonic kidney 293T (HEK293T) cells (Fig. S6*A*). In addition, similarly high levels of colocalization were observed between the GFP-ML1N*2 probe and LysoTracker (Fig. 1*F*), a probe for acidic organelles, or endogenous Lamp1 (Fig. 1*G*). No consistent PM localization was seen, although in some cells the probe is localized in patchy regions of PM (Fig. S8). In a proportion of certain cell types, the probe was also localized to the nucleus (Fig. 1*B* and Fig. S6*A*), a finding that was similarly observed for some other phosphoinositide probes (2, 15), and for tandem repeats of EGFP alone (22). Collectively, these results suggest that a significant pool of $PI(3,5)P_2$ resides on Lamp1-positive compartments.

We also investigated the colocalization of ML1N*2 with other endocytic markers. The early endosomal marker EEA1 showed significant colocalization with the probe (31.5 ± 2.4%, $n = 25$; Fig. 1 *H* and *K*), which is consistent with a previous observation that in fibroblasts, ~40% of Vac14 proteins colocalize with EEA1-positive compartments (8). A commonly used PI(3)P probe GFP-FYVE*2 (6) exhibited a high degree of colocalization with the mCherry-ML1N*2 probe (65.7 ± 3.4%, $n = 22$; Fig. 1 *I* and *K*, and Fig. S9), a reflection of the fact that PI(3)P is the primary precursor and metabolite of $PI(3,5)P_2$ (8, 11). Consistent with PIKfyve being the primary kinase responsible for the synthesis

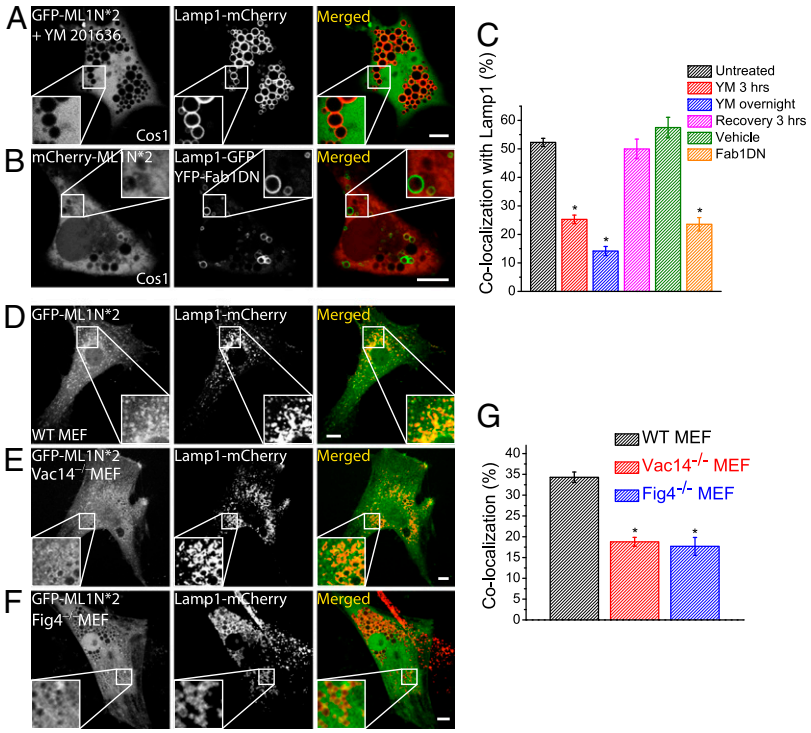

Fig. 2. Genetically or pharmacologically induced decreases in $PI(3,5)P_2$ levels diminish or abolish the vesicular localization of the ML1N*2 probe. (*A*) GFP-ML1N*2– and Lamp1-mCherry–transfected COS1 cells were treated with YM201636 (800 nM) overnight before confocal imaging analysis. Although Lamp1-positive compartments were dramatically enlarged, the GFP-ML1N*2 probe was primarily localized to the cytosol and was not found on enlarged vacuolar membranes. (*B*) The vesicular localization of the mCherry-ML1N*2 probe was significantly reduced in cells cotransfected with the 1-phosphatidylinositol-3-phosphate 5-kinase (Fab1)-DN construct. Images were taken 24 h posttransfection. (*C*) YM201636 treatment resulted in a progressive decrease in ML1N*2's colocalization with Lamp1. Washout of the drug in the culture medium led to a complete recovery of the colocalization. (*D*–*F*) The ML1N*2 probe exhibited an apparent vesicular localization pattern in WT (*D*), but not in $Vac14^{-/-}$ (*E*) or $Fig4^{-/-}$ (*F*) MEF cells. (*G*) The colocalization index between ML1N*2 and Lamp1 was significantly reduced in $Vac14^{-/-}$ and $Fig4^{-/-}$ MEFs. Error bars represent SEM; numbers of data points are given in the text. The asterisk indicates $P < 10^{-5}$. (Scale bar: 10 μm.)

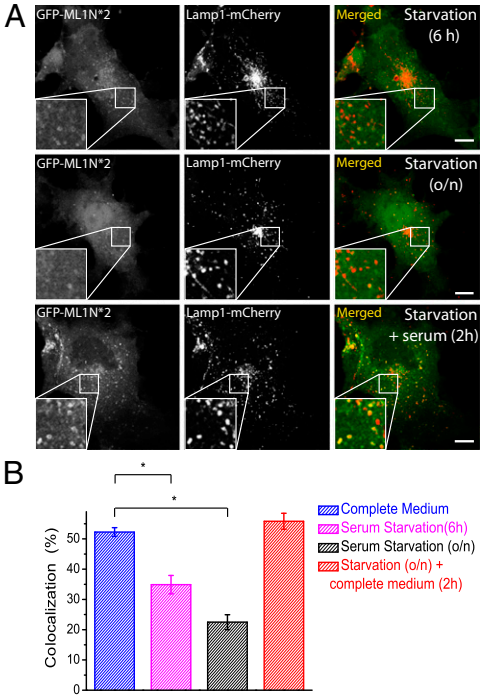

Fig. 3. Endolysosomal PI(3,5)P_2 levels are regulated by serum-derived factors. (*A*) In COS1 cells dually transfected with GFP-ML1N*2 and Lamp1-mCherry, serum starvation induced a progressive reduction in the colocalization of ML1N*2 and Lamp1. Readdition of complete medium rapidly (<2 h) restored the high degree of colocalization. (*B*) Serum-dependent colocalization of the ML1N*2 probe and Lamp1. Error bars represent SEM; numbers of data points are given in the text. The asterisk indicates $P < 10^{-5}$. (Scale bar: 10 μm.)

of PI(3,5)P_2, a high degree of colocalization between ML1N*2 and PIKfyve-YFP was observed on vesicular structures in COS1 cells (52.1 ± 4.2%, $n = 21$; Fig. 1 *J* and *K*).

Reducing PI(3,5)P_2 Levels Decreases or Abolishes the Endolysosomal Localization of the ML1N*2 Probe in Both Mammalian and Yeast Cells. The results presented thus far suggest that the endolysosomal localization of the probe is likely due to its binding to PI(3,5)P_2 located on endolysosomal membranes. To further test this possibility, we used several approaches to manipulate intracellular PI(3,5)P_2 levels to investigate whether the localization pattern of the probe changed in response to an increase or decrease in PI(3,5)P_2 levels. In mammalian cells, physiological stimuli that induce a robust elevation in PI(3,5)P_2 levels have not been established, although in some cell types PI(3,5)P_2 levels can be increased moderately (usually less than twofold) by certain types of extracellular stimulation, such as osmotic shock (23) or insulin application (24). Genetic and pharmacological tools to dramatically reduce PI(3,5)P_2 levels are available.

YM201636 is a widely used PIKfyve inhibitor that attenuates PI(3,5)P_2 production, resulting in enlarged endolysosomes (25). In COS1 cells coexpressing the GFP-ML1N*2 probe and Lamp1-mCherry, YM201636 treatment dramatically reduced the colocalization of the probe with Lamp1 to 14.2 ± 1.6% ($n = 47$; Fig. 2 *A* and *C*). Similar results were seen in NIH 3T3 cells (Fig. S8). The effect of YM201636 was reversible because the colocalization index returned to the normal level 3 h after drug removal (47.7 ± 3.0%, $n = 13$; Fig. 2*C*). Moreover, the effect of YM201636 was specific because the vesicular localization of the PI(3)P probe GFP-FYVE*2 remained unaffected (Fig. S9). Note that, in the presence of YM201636, some of the ML1N-2*-GFP probe was still observed on a small number of vacuoles (Fig. S8), raising the possibility that in the absence of PI(3,5)P_2, the ML1N-2*-GFP probe recognizes another epitope, either a protein or lipid. Interestingly, when purified GST-GFP-ML1N*2 proteins were exogenously applied to the fixed cells, GFP fluorescence exhibited a vesicular localization pattern and significant colocalization with Lamp1, which was abolished by YM 201636 treatment for 30 min (Fig. S10). These results suggested that the probe binds directly to the Lamp1-positive membranes in a YM201636-sensitive manner.

The kinase activity of PIKfyve can also be inhibited by overexpression of dominant-negative (DN) PIKfyve (26). In COS1 cells cotransfected with YFP-PIKfyve-DN, mCherry-ML1N*2, and Lamp1-GFP, enlarged vacuoles were seen (Fig. 2*B*) with an accompanying, profound decrease in the colocalization between Lamp1 and the probe (23.6 ± 2.4%, $n = 25$; Fig. 2*C*).

Although PIKfyve knockout (KO) mice are embryonic lethal (11), Vac14 and Fig4 KO mice can survive postnatally with reduced intracellular PI(3,5)P_2 levels (~50% of WT control) (9, 10). In both Vac14 KO and Fig4 KO MEF cells, the colocalization between GFP-ML1N*2 and Lamp1 was significantly reduced compared with WT MEF cells (18.8 ± 1.3%, $n = 38$, and 17.7 ± 2.2%, $n = 29$, for Vac14 and Fig4 KO MEFs, respectively, vs. 34.3 ± 1.3%, $n = 41$, for WT cells; Fig. 2 *D*–*G*). Taken together, these results suggest that the endolysosomal localization of the probe was dependent on the activity of PIKfyve/Fab1 and that the probe was capable of detecting changes in intracellular PI(3,5)P_2 levels.

Because genetic means of altering PI(3,5)P_2 levels are well established in the yeast system (7, 20, 27), we also performed the assay in yeast cells. In WT yeast cells, the GFP-ML1N*2 probe showed a very clear vacuolar localization, as shown by its colocalization with the FM4-64 dye, a fluorescent marker of vacuolar membranes (Fig. S11). Hypertonic shock activation of Fab1-mediated PI(3,5)P_2 production (20) further increased the vacuolar localization of the probe (Fig. S11). Yeast cells lacking *fab1* (yeast ortholog of PIKfyve; *fab1Δ*) contain an undetectable level of PI(3,5)P_2 with a characteristic enlarged vacuole phenotype (7, 20, 27). In *fab1Δ* yeast cells, the vacuolar localization was dramatically diminished (Fig. S11). These results suggest that the vacuolar localization pattern of the probe in yeast cells is most likely mediated by PI(3,5)P_2. Unlike mammalian cells (Fig. 1), the GFP-ML1N*2 probe also showed consistent, evenly distributed PM localization in both WT and *fab1Δ* yeast strains (Fig. S11). Prominent PM localization was seen (Fig. S11) even with the GFP-ML1N*1 probe in both WT and PI(4,5)P_2-deficient Mss4 mutant (28) yeast cells (Fig. S11). Thus, the PM localization of the probe in yeast is likely unrelated to PI(3,5)P_2 or PI(4,5)P_2. This may compromise the use of the probe for yeast studies.

Endolysosomal PI(3,5)P_2 Levels Are Regulated by Serum-Derived Factors. We used the probe to track the dynamic and regulatory changes of PI(3,5)P_2 in living cells. In 3T3L1 adipocytes, insulin has been shown to induce a modest increase in PI(3,5)P_2 levels in serum-starved cells (19, 26). Likewise, serum-derived factors such as hormones and growth factors would regulate the levels of PI(3,5)P_2 and other phosphoinositides in other cell types (12). Consistently, serum starvation elicited a striking change in the pattern of the probe localization in COS1 cells. Under normal conditions, the GFP-ML1N*2 probe was seen on Lamp1-positive vacuole membranes as intensely bright circles or dots (depending on the vacuole size) (Fig. 1*B*). However, in COS1 cells serum-starved for 6 h (Fig. 3*A*, *Top*) or overnight for 18 h (Fig. 3*A*, *Middle*), the percentage of the colocalization between Lamp1 and the ML1N*2 probe decreased significantly (34.9 ± 3.0%, $n = 23$, for 6 h; 22.9 ± 2.5%, $n = 24$, for 18 h; Fig. 3*B*). Furthermore, the relative intensity of the probe on the positive vacuoles was greatly reduced compared with serum-replete or normal conditions. When cells were replenished with serum for 2 h, both colocalization (55.8 ± 2.6%, $n = 25$) and signal intensity returned to normal levels (Fig. 3*A*, *Bottom*). Thus, intracellular PI(3,5)P_2 levels are regulated by unknown

hormones or growth factors in the serum, the identification of which can be facilitated by the use of the ML1N*2 probe.

PI(3,5)P_2 Dynamics in Relation to Endolysosomal Membrane Fusion in Mammalian Cells. PI(3,5)P_2 is a key regulator of membrane trafficking (membrane fusion and fission) in LELs, and PI(3,5)P_2 deficiency causes endolysosomal enlargement due to trafficking defects (7). Because PI(3,5)P_2 directly activates lysosomal TRPML1 channels, it was hypothesized that PI(3,5)P_2 elevation may induce lysosomal Ca^{2+} release to trigger endolysosomal membrane fusion/fission (13, 20, 29). To visualize PI(3,5)P_2 dynamics in relation to membrane fusion/fission in live cells, we performed time-lapse confocal imaging in COS1 cells that were dually transfected with GFP-ML1N*2 and Lamp1-mCherry, with Lamp1-mCherry revealing the fusion events and GFP-ML1N*2 tracking PI(3,5)P_2 dynamics. Due to the small size (<0.5 μm) of most Lamp1-positive compartments, we were not able to clearly resolve membrane fusion/fission events for these vesicles due to the limitation imposed by the image resolution. For larger vesicles (>0.5–1 μm for both vacuoles undergoing fusion), however, the naturally occurring fusion rate appeared to be very low (~0.01 events per cell per min). Nevertheless, in the few observations we made, a rapid and robust increase in the vacuolar GFP fluorescence was detected immediately before fusion of the two Lamp1-positive vacuoles occurred (Fig. 4 *A* and *C*, and Movie S1). The intensity of the probe peaked at the time of fusion, and then gradually decreased over time (Fig. 4*B*). In contrast, mCherry-Lamp1 intensity and cytoplasmic GFP-ML1N*2 fluorescence intensity remained relatively constant, suggesting that the increase in the vacuolar GFP-ML1N*2 fluorescence [hence PI(3,5)P_2 level] was the cause, and not the result, of membrane fusion. These results suggest that PI(3,5)P_2 is rapidly produced to reach a high level before fusion events.

To facilitate the detection of fusion events between large vacuoles, we treated the cells with an acetate Ringer's solution for 20–30 min. Treatment with acetate Ringer's has long been known to cause cytoplasmic acidification that induces vacuolar fragmentation and the subsequent redistribution of vacuoles to the periphery of the cells, the mechanism of which is poorly understood (30, 31). Upon removal of acetate Ringer's solution, the lysosomes quickly regain their size through increased fusion frequency, typically in 10–30 min (30, 31). In COS1 cells that were dually transfected with GFP-ML1N*2 and Lamp1-mCherry, withdrawal of the acetate Ringer's solution resulted in an increased (~20-fold) rate of fusion between large vacuoles (~0.17 events per cell per min). All vacuoles undergoing fusion had a much higher (164.4 ± 1.5%, n = 22) probe intensity on the vacuolar membranes than the cytosolic background at the time of fusion. Based on the PI(3,5)P_2 responses, the fusogenic vacuoles could be classified into two groups. The first group (~45% of all events) had significant increases (>20%) in the membrane intensity within 1 min of prefusion (Fig. 4 *D* and *E*, upper panels, and Movie S2), whereas the second group (~55% of all events) exhibited little or no increase (Fig. 4*E* and Movie S3). Interestingly, the basal fluorescence intensity of the probe in the second group was significantly higher than that of the first group (Fig. 4 *D*–*F*). These results suggest that recovery from the acetate Ringer's treatment uses PI(3,5)P_2-dependent mechanisms to facilitate membrane fusion between LELs.

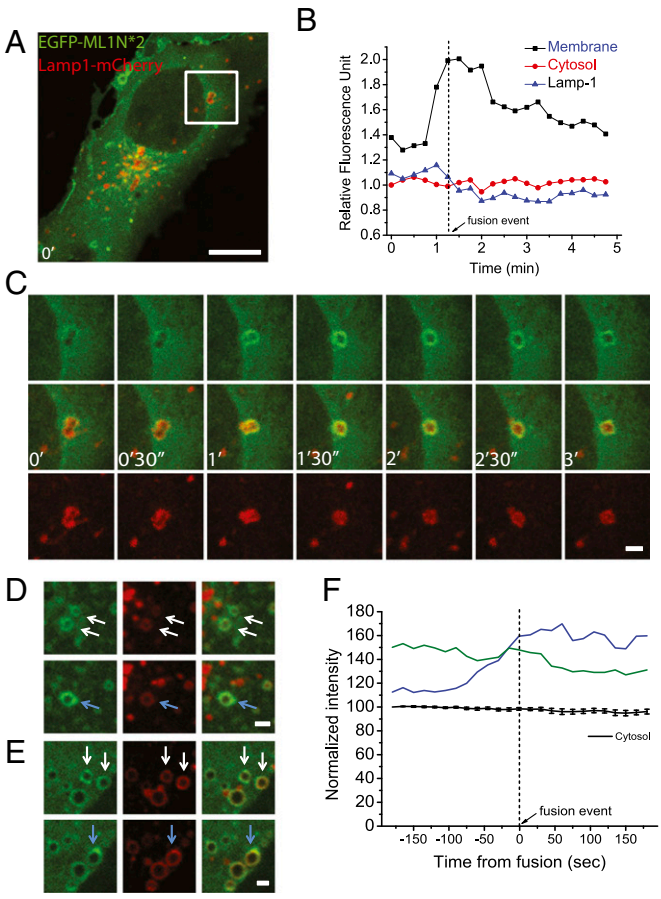

Fig. 4. PI(3,5)P_2 is transiently increased immediately before membrane fusion in LELs. (*A*–*C*) Time-lapse live imaging of COS1 cells that were dually transfected with GFP-ML1N*2 and Lamp1-mCherry. (*A*) Image of a COS1 cell immediately before membrane fusion between two Lamp1-positive vacuoles occurred (highlighted in the white box). (*B*) Time-dependent changes in the fluorescence intensities of GFP and mCherry for the selected region (white box, *A*). (*C*) Series of images of the selected region at corresponding time points as in *B*. For a 4-min track period, one fusion event between two vacuoles occurred between every 1 min and 1 min 15 s (*D* and *E*) GFP-ML1N*2 and Lamp1-mCherry dually transfected COS1 cells were treated with acetate Ringer's solution for 30 min and then subjected to live imaging for 5–20 min after being returned to the normal Ringer's solution. Approximately one-half of the vacuoles (45% of the 22 monitored events; *D*) exhibited a significant increase (>20% of the baseline membrane intensity) in their membranous PI(3,5)P_2 levels immediately before fusion, whereas the other half (55%; *E*) had little or no changes. The white and blue arrows mark vacuoles prefusion and postfusion, respectively. (*F*) Changes in vacuolar PI(3,5)P_2 levels in relation to fusion events. The fluorescent intensity of GFP-ML1N*2 was normalized to the cytosolic intensity at time 0, and two representative traces are shown; the vertical dotted line indicates the time when the fusion took place. The cytosolic intensity of the probe remained relatively constant over the time period of the live-imaging experiment. [Scale bar: 10 μm (for *A*) and 2 μm (for *C* and *D*).]

Discussion

Although the importance of PI(3,5)P_2 in endolysosomal membrane trafficking is well accepted, the dynamics and localization of PI(3,5)P_2 are unclear, largely due to the lack of a method to directly monitor PI(3,5)P_2 levels in intact cells. In the present study, we report a fully characterized PI(3,5)P_2 fluorescent probe that can be used to track in situ PI(3,5)P_2 dynamics. Our PI(3,5)P_2 fluorescent probe, consisting of two repeats of the cytosolic N terminus of the lysosomal channel TRPML1, responds specifically to changes in the intracellular PI(3,5)P_2 level and localization, as indicated by the following key findings. First, the probe is colocalized with the PI(3,5)P_2-synthesizing enzyme complex. Second, charge-neutralizing mutations in the putative PI(3,5)P_2 binding domain abolish the vacuolar localization of the probe. Third, increasing or decreasing PI(3,5)P_2 levels in both yeast and mammalian cells cause corresponding changes in the vacuolar localization of the probe. Thus, the probe can reliably detect PI(3,5)P_2 in living cells.

The predominantly LEL localization of the probe is somewhat unexpected. Although PI(3,5)P_2, unlike other phosphoinositides, activates TRPML1 in the nanomolar range, PI(4,5)P_2 and PI(3,4,5)P_3, two PM-localized phosphoinositides, inhibit TRPML1

NEUROSCIENCE

(21). Although very weakly, the in vitro binding assays demonstrated that ML1N (20) and also its tandem dimer bound to PI(4,5)P_2 and PI(3,4,5)P_3. However, no consistent PM localization was detected in the mammalian cell types that we tested, although in some cell types patchy PM localization was observed. One plausible explanation is that the affinity of TRPML1 for PI(3,5)P_2 is 5- to 10-fold higher than that of PI(4,5)P_2 and PI(3,4,5)P_3 (21). Alternatively, the probe overexpression might have resulted in PI(3,5)P_2 enrichment in LELs by protecting them from phosphatase-mediated degradation, as was observed for the PI(4,5)P_2 probe, where the probe expression attenuated the PLC hydrolysis of PI(4,5)P_2 (32). It is also likely that ML1N contains additional PI(3,5)P_2-dependent or -independent motifs that specifically strengthen the LEL localization of the probe. Similar observations have been reported for other phosphoinositide probes, including the PI(4)P probe (2, 15, 17). Although not identified yet, an additional recruiting mechanism may play a crucial and permissive role in the LEL localization of the PI(3,5)P_2 probe. Nevertheless, such putative dual recruiting mechanism would not prevent the use of the current probe to detect PI(3,5)P_2 dynamics in LELs. Probe localization in other compartments, however, needs to be cautiously interpreted, as other phosphoinositides may be much more abundant than PI(3,5)P_2 despite their very weak binding affinities. In addition, the weak binding of the tandem probe to PI(5)P could be potentially problematic, as this lipid is also known to be present in the late endocytic compartments of mammalian cells, and is produced from the PI(3,5)P_2 generated by PIKfyve (12). Because the production of these two phosphoinositides are linked, and their biological roles have not been clearly separated, the probe may also detect the changes of the PI(5)P, similar to the case of detection of PI(3,4)P_2 and PI(3,4,5)P_3 with the AKT-PH probe (15).

Due to the lack of an effective PI(3,5)P_2 fluorescent probe, the measurement of intracellular PI(3,5)P_2 levels has thus far been restricted to indirect approaches such as radiolabeled HPLC, a technique that requires lengthy protocols, and provides no information about subcellular localization and real-time dynamics. By using the PI(3,5)P_2 probe that we have developed and characterized, we have shown that PI(3,5)P_2 elevation occurs immediately before endolysosomal fusion, highlighting the role of PI(3,5)P_2 in regulating endolysosomal fusion. TRPML1 is a lysosomal channel that mediates Ca^{2+} release from the lysosomal lumen (13) to trigger membrane fusion in LELs (29). Because PI(3,5)P_2 elevation may activate TRPML1-mediated Ca^{2+} release (13, 20), it is likely that PI(3,5)P_2 is the trigger for fusion between lysosomes and various other compartments (e.g., late endosomes, autophagosomes, phagosomes, and plasma membrane). We have recently shown that PI(3,5)P_2 elevation occurs during lysosomal exocytosis and phagosome formation (33). With the aid of high-resolution live imaging in combination with genetic and pharmacological approaches, the PI(3,5)P_2 probe will prove invaluable in studying the regulation of PI(3,5)P_2 dynamics in signal transduction and membrane trafficking.

Materials and Methods

For fixed samples, cells were fixed and immunostained following a standard protocol, and then imaged with a Leica confocal microscope. Live imaging was performed with an Olympus Spindisk confocal microscope. Images were analyzed with ImageJ software. Colocalization was performed with the Colocalization Plug-in of ImageJ. See *SI Materials and Methods* for details of experimental procedures.

ACKNOWLEDGMENTS. We are grateful to Dongbiao Shen, Titus Franzmann, and Stefan Walter for assistance; Drs. William Brown and Jennifer Meagher from the Center for Structural Biology, Life Sciences Institute, for the optimization of the purification of GST-fusion protein; Drs. Harald Stenmark for the FYVE*2-GFP construct; and Abigail Garrity and Richard Hume for comments on an earlier version of the manuscript. We appreciate the encouragement and helpful comments of other members of the H.X. laboratory. This work was supported by National Institutes of Heath Grants R01 NS062792 (to H.X.) and R01 GM50403 (to L.S.W.).

1. Di Paolo G, De Camilli P (2006) Phosphoinositides in cell regulation and membrane dynamics. *Nature* 443(7112):651–657.
2. Lemmon MA (2008) Membrane recognition by phospholipid-binding domains. *Nat Rev Mol Cell Biol* 9(2):99–111.
3. Stauffer TP, Ahn S, Meyer T (1998) Receptor-induced transient reduction in plasma membrane PtdIns(4,5)P2 concentration monitored in living cells. *Curr Biol* 8(6): 343–346.
4. Suh BC, Hille B (2008) PIP2 is a necessary cofactor for ion channel function: How and why? *Annu Rev Biophys* 37:175–195.
5. Lee WL, Mason D, Schreiber AD, Grinstein S (2007) Quantitative analysis of membrane remodeling at the phagocytic cup. *Mol Biol Cell* 18(8):2883–2892.
6. Gillooly DJ, et al. (2000) Localization of phosphatidylinositol 3-phosphate in yeast and mammalian cells. *EMBO J* 19(17):4577–4588.
7. Dove SK, Dong K, Kobayashi T, Williams FK, Michell RH (2009) Phosphatidylinositol 3,5-bisphosphate and Fab1p/PIKfyve underPPIn endo-lysosome function. *Biochem J* 419(1):1–13.
8. Zhang Y, et al. (2012) Modulation of synaptic function by VAC14, a protein that regulates the phosphoinositides PI(3,5)P(2) and PI(5)P. *EMBO J.* 31(16):3442–3456.
9. Chow CY, et al. (2007) Mutation of FIG4 causes neurodegeneration in the pale tremor mouse and patients with CMT4J. *Nature* 448(7149):68–72.
10. Zhang Y, et al. (2007) Loss of Vac14, a regulator of the signaling lipid phosphatidylinositol 3,5-bisphosphate, results in neurodegeneration in mice. *Proc Natl Acad Sci USA* 104(44):17518–17523.
11. Ikonomov OC, et al. (2011) The phosphoinositide kinase PIKfyve is vital in early embryonic development: Preimplantation lethality of PIKfyve−/− embryos but normality of PIKfyve+/− mice. *J Biol Chem* 286(15):13404–13413.
12. Zolov SN, et al. (2012) In vivo, Pikfyve generates PI(3,5)P_2, which serves as both a signaling lipid and the major precursor for PI5P. *Proc Natl Acad Sci USA* 109(43): 17472–17477.
13. Shen D, et al. (2012) Lipid storage disorders block lysosomal trafficking by inhibiting a TRP channel and lysosomal calcium release. *Nat Commun* 3:731.
14. Wang X, et al. (2012) TPC proteins are phosphoinositide-activated sodium-selective ion channels in endosomes and lysosomes. *Cell* 151(2):372–383.
15. Balla T (2007) Imaging and manipulating phosphoinositides in living cells. *J Physiol* 582(Pt 3):927–937.
16. Halet G (2005) Imaging phosphoinositide dynamics using GFP-tagged protein domains. *Biol Cell* 97(7):501–518.
17. Carlton JG, Cullen PJ (2005) Coincidence detection in phosphoinositide signaling. *Trends Cell Biol* 15(10):540–547.
18. Tsuruta F, Green EM, Rousset M, Dolmetsch RE (2009) PIKfyve regulates CaV1.2 degradation and prevents excitotoxic cell death. *J Cell Biol* 187(2):279–294.
19. Bridges D, et al. (2012) Phosphatidylinositol 3,5-bisphosphate plays a role in the activation and subcellular localization of mechanistic target of rapamycin 1. *Mol Biol Cell* 23(15):2955–2962.
20. Dong XP, et al. (2010) PI(3,5)P(2) controls membrane trafficking by direct activation of mucolipin Ca^{2+} release channels in the endolysosome. *Nat Commun* 1:38.
21. Zhang X, Li X, Xu H (2012) Phosphoinositide isoforms determine compartment-specific ion channel activity. *Proc Natl Acad Sci USA* 109(28):11384–11389.
22. Seibel NM, Eljouni J, Nalaskowski MM, Hampe W (2007) Nuclear localization of enhanced green fluorescent protein homomultimers. *Anal Biochem* 368(1):95–99.
23. Hill EV, Hudson CA, Vertommen D, Rider MH, Tavaré JM (2010) Regulation of PIKfyve phosphorylation by insulin and osmotic stress. *Biochem Biophys Res Commun* 397(4): 650–655.
24. Shisheva A, Rusin B, Ikonomov OC, DeMarco C, Sbrissa D (2001) Localization and insulin-regulated relocation of phosphoinositide 5-kinase PIKfyve in 3T3-L1 adipocytes. *J Biol Chem* 276(15):11859–11869.
25. Jefferies HB, et al. (2008) A selective PIKfyve inhibitor blocks PtdIns(3,5)P(2) production and disrupts endomembrane transport and retroviral budding. *EMBO Rep* 9(2):164–170.
26. Ikonomov OC, Sbrissa D, Shisheva A (2009) YM201636, an inhibitor of retroviral budding and PIKfyve-catalyzed PtdIns(3,5)P2 synthesis, halts glucose entry by insulin in adipocytes. *Biochem Biophys Res Commun* 382(3):566–570.
27. Duex JE, Nau JJ, Kauffman EJ, Weisman LS (2006) Phosphoinositide 5-phosphatase Fig 4p is required for both acute rise and subsequent fall in stress-induced phosphatidylinositol 3,5-bisphosphate levels. *Eukaryot Cell* 5(4):723–731.
28. Desrivières S, Cooke FT, Parker PJ, Hall MN (1998) MSS4, a phosphatidylinositol-4-phosphate 5-kinase required for organization of the actin cytoskeleton in *Saccharomyces cerevisiae*. *J Biol Chem* 273(25):15787–15793.
29. Shen D, Wang X, Xu H (2011) Pairing phosphoinositides with calcium ions in endolysosomal dynamics: Phosphoinositides control the direction and specificity of membrane trafficking by regulating the activity of calcium channels in the endolysosomes. *Bioessays* 33(6):448–457.
30. Heuser J (1989) Changes in lysosome shape and distribution correlated with changes in cytoplasmic pH. *J Cell Biol* 108(3):855–864.
31. Durchfort N, et al. (2012) The enlarged lysosomes in beige j cells result from decreased lysosome fission and not increased lysosome fusion. *Traffic* 13(1):108–119.
32. Várnai P, Balla T (1998) Visualization of phosphoinositides that bind pleckstrin homology domains: Calcium- and agonist-induced dynamic changes and relationship to myo-[^{3}H]inositol-labeled phosphoinositide pools. *J Cell Biol* 143(2):501–510.
33. Samie M, et al. (2013) A TRP channel in the lysosome regulates large particle phagocytosis via focal exocytosis. *Dev Cell* 26(5):511–524.

Supporting Information

Li et al. 10.1073/pnas.1311864110

SI Materials and Methods

Molecular Biology. Tandem repeats of the transient receptor potential Mucolipin 1 (TRPML1) (accession number CCDS22063.1 in National Center for Biotechnology Information cDNA database) N-terminal segment (residues 1–68) were subcloned from mouse cDNA into a pEGFPC3 (Clontech) plasmid by using the following two pairs of primers: F1: GAAGATCTCA CCATGG-CCAC CCCG; R1: CGGAATTCGC AGCATCAGCT TGCAG; F2: CGGAATTCTC ACCATGGCCA CCCC; R2 CGGGA-TCCAG CATCAGCTTG CAG. For the mCherry-ML1N*2 construct, mCherry was inserted into the GFP-ML1N*2 construct from the pmCherry-C1 plasmid (Clontech) to replace GFP by using the following primers: F: CATCAAGTGT ATCA-TATGCC; R: GAAGATCTAG TCCGGA-CTTG TACAG. The ML1N-7Q*2 and ML1N-2A*2 mutants were generated by site-directed mutagenesis with Pfu Turbo polymerase (Stratagene). Yeast expression constructs were made by insertion of ML1N amplified from the GFP-ML1N*2 plasmid into the pVT102U-GFP vector (1). A glutathione S-transferase (GST)-fusion construct was made by inserting the GFP-ML1N*2 fragment into the pGEX-4T1 vector (GE Healthcare). The Lamp1-mCherry construct was made by insertion of lysosomal-associated membrane protein 1 (Lamp1) cDNA into pcDNA3.1 (Invitrogen) followed by fusion of mCherry with the C terminus of Lamp1. All constructs were confirmed by sequencing.

GST-Fusion Protein Purification. To purify GST-GFP-ML1N*2, *Escherichia coli* strain BL-21 supplemented with pRareCDF (optimizing for mammalian codon distribution) was transformed with pGEX4T1-GFP-ML1N*2. Bacteria were inoculated at 37 °C in Terrific Broth medium containing spectinomycin and ampicillin. Once the OD of the culture reached ∼2, cells were equilibrated to room temperature and protein expression was induced with 250 μM isopropyl β-D-1-thiogalactopyranoside for 2 h. Cells were then pelleted and resuspended with PBS containing 0.5 mM EDTA, 0.1 mg/mL lysozyme, and 1% (vol/vol) protease inhibitor mixture (P8849; Sigma). Cells were then lysed by sonication and centrifuged. The GST-fusion proteins in the supernatant were concentrated using glutathione Sepharose beads (GE Healthcare). After extensive washes with PBS, purified proteins were eluted with elution buffer (20 mM glutathione, 150 mM NaCl in 50 mM Tris, pH 8.0).

Liposome Binding Assay. Phosphoinositide-containing liposomes (PIPosomes) from Echelon Biosciences were used for the assay. Twenty microliters of liposomes were diluted in 1 mL of binding buffer (150 mM NaCl, 0.05% Nonidet P-40 in 50 mM Tris, pH 7.5) containing 3 μg of GST-GFP-ML1N*2. After 10 min of incubation, liposomes were pelleted at 16,000 × *g* for 10 min. Supernatants were carefully removed and liposomes were resuspended with 1 mL of binding buffer. After six washes, the bound fractions were analyzed by Western blot using anti-GST antibodies.

To estimate the affinity (K_d) of phosphatidylinositol 3,5-bisphosphate [PI(3,5)P_2]-probe binding, liposomes containing 30–3,000 pmol of PI(3,5)P_2 or 2 nmol of control lipids without PI(3,5)P_2 were incubated with various concentrations of the purified GST-GFP-ML1N*2 proteins in 100 μL of binding buffer. The mixture was incubated for 1 h with gentle rotation. After 10 μL of the mixture was separated as input, the liposomes were pelleted at 16,000 × *g* for 15 min. The supernatant was then carefully separated as the unbound fraction. Protein concentrations from input and unbound fractions were measured by absorbance at 280 nm and Western blot analysis.

Lipid Strip Binding Assay. PIP-strip was purchased from Echelon Biosciences (P-6001), containing 15 different lipid species, including all 7 phosphoinositides. The strip was first blocked with PBST [containing 3% (wt/vol) BSA] for 1 h, incubated with 0.2 μg/mL GST-GFP-ML1N*2 for 1 h, and then washed six times with the blocking buffer. Bound proteins were recognized with anti-GST antibodies (Sigma; G1160) and detected with goat anti-mouse HRP-conjugated secondary antibodies (Invitrogen; 62-6520).

PIP Beads Binding Assay. Fifty microliters of 50% (vol/vol) phosphoinositide-containing beads (Echelon Biosciences) were incubated with 1 mL of binding buffer (150 mM NaCl, 0.25% Nonidet P-40 in 50 mM Tris, pH 7.5) containing 5 μg of GST-GFP-ML1N*2. After 2 h of incubation, beads were pelleted at 500 × *g* for 5 min, and beads were resuspended with 1 mL of binding buffer. After five washes, the bound fractions were analyzed by Western blot using anti-GST antibodies.

PI(3,5)P_2 Detection Using Purified GST-GFP-ML1N*2 Proteins. Lamp1-transfected cells were fixed with 4% (wt/vol) paraformaldehyde (PFA), blocked with PBST [containing 3% (wt/vol) BSA] for 2 h, incubated with 5 μg/mL GST-GFP-ML1N*2 in the blocking buffer for 2 h, and then subjected to fluorescence microscopy.

Mammalian Cell Culture. Mammalian cells were cultured in a 37 °C, 5% CO_2 incubator. Mouse embryonic fibroblasts (MEFs) were isolated and cultured as described previously (1). (Animals were used under approved animal protocols and Institutional Animal Care Guidelines at the University of Michigan). Cells were cultured with DMEM (Invitrogen) supplemented with 10% (vol/vol) FBS (Gemini). All other mammalian cell types (CHO, COS1, and HEK293T) were cultured with DMEM F12 (Invitrogen) supplemented with 10% (vol/vol) FBS. For the delivery of the plasmids into the cells, MEF cells were electroporated by using an Invitrogen Neon electroporation kit; all other mammalian cells were transfected by using Lipofectamine 2000 (Invitrogen). Cells were typically imaged 24 h posttransfection. Serum starvation was performed with three washes of PBS to completely remove serum. Cells were then incubated with the respective culture medium without serum for the indicated periods. Acetate Ringer's solution (2, 3) contained the following (in mM): 80 NaCl, 70 CH_3COOH, 5 KCl, 2 $CaCl_2$, 1 $MgCl_2$, 2 NaH_2PO_4, 10 Hepes, 10 Mes, and 10 glucose (pH adjusted to 6.9 with NaOH). Standard Ringer's solution contained the following (in mM): 145 NaCl, 5 KCl, 2 $CaCl_2$, 1 $MgCl_2$, 10 Hepes, 10 Mes, and 10 glucose (pH adjusted to 7.4 with NaOH).

Yeast Cell Culture. WT yeast (strain LWY7235, *MATa leu2,3-112 ura3-52*, *his3-Δ200*, *trp1-Δ901*, *lys2-Δ801*, *suc2-Δ9*); *fab1Δ* yeast (strain LWY2055, *MATa leu2,3-112 ura3-52*, *his3-Δ200*, *trp1-Δ901*, *lys2-Δ801*, *suc2-Δ9, fab1Δ::LEU2*); *mss4^{ts}* yeast (strain SD102, *MAT a leu2–3,112 ura3–52 trp1 his4 rme1 HMLa his3D HIS4 mss4::HIS3MX6/YCplac111::mss4–2ts*) were cultured in yeast extract peptone dextrose medium and transformed with plasmids using a Li-acetate protocol. Transformants were grown in selective synthetic defined (SD) minimal medium (1). For microscopy imaging, yeast cells were labeled for 1 h with FM4-64 dye (Biotium) (12 μg of FM4-64 in 0.25 OD_{600} units of yeast cells, in 250 μL), and chased for 3 h in selective SD medium (1). Cells were then pelleted and resuspended in the SD medium for imaging.

Confocal Microscopy. For fixed samples, cells were fixed and immunostained following a standard protocol. Briefly, cells were fixed with 4% (wt/vol) PFA for 30 min, blocked with 1% BSA for 2 h, incubated with primary antibody overnight, and stained with fluorescent secondary antibody for 1 h. Cells were then imaged with a Leica confocal microscope. For live samples, cells were washed with DMEM F12 medium without phenol red (Invitrogen) to reduce background fluorescence. Live imaging was performed with an Olympus Spindisk confocal microscope with a heated chamber to maintain the temperature at ~37 °C during imaging. Wavelengths used for each channel are (excitation/emission in nm): 405/447 (DAPI), 488/525 (GFP), and 561/607 (mCherry).

Imaging Analysis. Images were analyzed with ImageJ software (4). For colocalization analysis, images were first split into separate color channels. The red and green channels were then thresholded on a regional basis, with the threshold being 50% above the average background intensity in the nearby cytosolic regions. Colocalization was performed with the Colocalization Plug-in of ImageJ. The percentage of colocalization was defined as the [total number of pixels that are positive for both channels/total number of pixels that are positive for the channel other than the probe (e.g., Lamp1)] × 100%. For the measurement of the change in the vacuolar fluorescence intensity, the vacuolar membrane area was selected by masking from the Lamp1-mCherry channel. The vacuolar probe intensity was defined as the average intensity of both vacuole membranes (before fusion) or the average intensity on the membrane of the fused vacuole.

Endolysosomal Electrophysiology. Endolysosomal electrophysiology was performed in isolated enlarged endolysosomes through a modified patch-clamp method, as described previously (1, 5–7). Briefly, cells overexpressing mouse TRPML1 or its mutants were treated with 1 μM vacuolin-1 for at least 2 h or for up to 12 h. Enlarged vacuoles (up to 5 μm) were manually isolated with a patch pipette, and then whole-endolysosome voltage-clamp recordings were performed. After formation of a gigaseal, capacitance transients were compensated. The vacuolar membrane was ruptured with a series of voltage steps. The whole-endolysosome configuration was verified by the reappearance of capacitance transients after break-in. Whole-endolysosomal currents were elicited by repeated voltage ramps from −120 to 120 mV (400 ms) with an interval of 2 s between ramps. The pipette (luminal) solution was a modified Tyrode's solution containing the following (in mM): 145 NaCl, 5 KCl, 2 $CaCl_2$, 1 $MgCl_2$, 10 Hepes, 10 Mes, and 10 glucose (pH adjusted with NaOH to pH 4.6). The bath (internal/cytoplasmic) solution contained the following (in mM): 140 K-gluconate, 4 NaCl, 1 EGTA, 2 $MgCl_2$, 0.39 $CaCl_2$, and 20 Hepes (pH adjusted with KOH to 7.2; free $[Ca^{2+}]_i$ ~ 100 nM). All bath solutions were applied via a perfusion system that allowed a complete solution exchange within a few seconds. Data were collected with an Axopatch 2A patch-clamp amplifier, Digidata 1440, and pClamp 10.2 software (Axon Instruments). Whole-endolysosome currents were digitized at 10 kHz and filtered at 2 kHz. All experiments were conducted at room temperature (21–23 °C), and all recordings were analyzed with pClamp 10.2 and Origin 8.0 (OriginLab).

Chemicals and Reagents. The PIKfyve inhibitor YM201636 (8) was purchased from Symansis. Mouse anti-Lamp1 antibody was purchased from the Developmental Studies Hybridoma Bank (1D4B). Monoclonal anti-GST antibody was purchased from Sigma (G1160).

Data Analysis. Statistical data are presented as the mean ± SEM. The quantifications shown in figures were performed for a total number (n) of individual cells for each group from at least three independent experiments. Statistical comparisons were made with a Student t test. Asterisks in the figures generally representing values of $P < 1 \times 10^{-5}$. A value of $P < 0.01$ was considered statistically significant.

1. Dong XP, et al. (2010) PI(3,5)P(2) controls membrane trafficking by direct activation of mucolipin Ca^{2+} release channels in the endolysosome. *Nat Commun*, 10.1038/ncomms1037.
2. Heuser J (1989) Changes in lysosome shape and distribution correlated with changes in cytoplasmic pH. *J Cell Biol* 108(3):855–864.
3. Durchfort N, et al. (2012) The enlarged lysosomes in beige j cells result from decreased lysosome fission and not increased lysosome fusion. *Traffic* 13(1):108–119.
4. Schneider CA, Rasband WS, Eliceiri KW (2012) NIH Image to ImageJ: 25 years of image analysis. *Nat Methods* 9(7):671–675.
5. Shen D, et al. (2012) Lipid storage disorders block lysosomal trafficking by inhibiting a TRP channel and lysosomal calcium release. *Nat Commun* 3:731.
6. Wang X, et al. (2012) TPC proteins are phosphoinositide- activated sodium-selective ion channels in endosomes and lysosomes. *Cell* 151(2):372–383.
7. Zhang X, Li X, Xu H (2012) Phosphoinositide isoforms determine compartment-specific ion channel activity. *Proc Natl Acad Sci USA* 109(28):11384–11389.
8. Jefferies HB, et al. (2008) A selective PIKfyve inhibitor blocks PtdIns(3,5)P(2) production and disrupts endomembrane transport and retroviral budding. *EMBO Rep* 9(2):164–170.

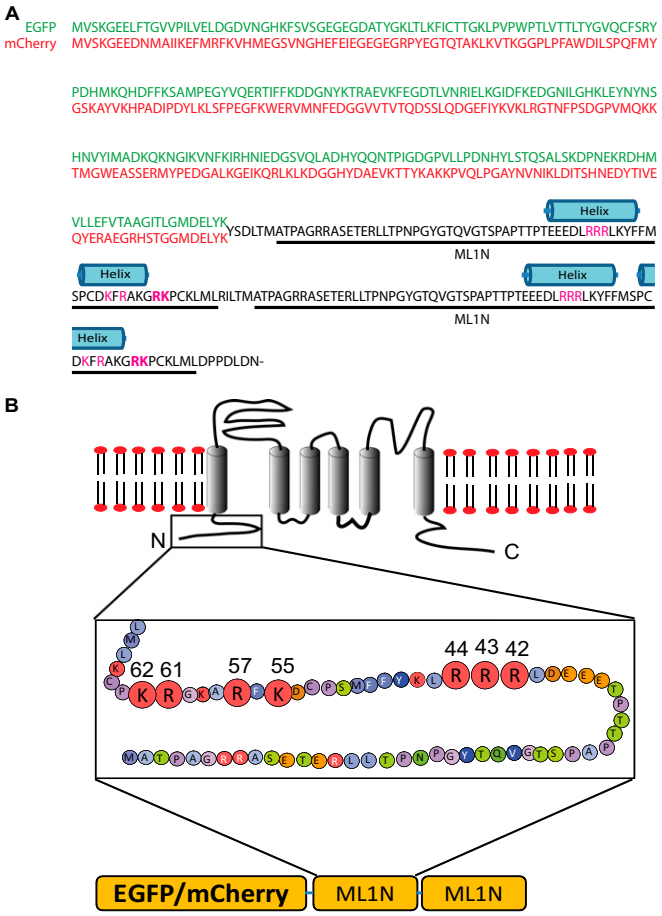

Fig. S1. Primary amino acid sequence and cartoon illustration of the ML1N*2 probe. (*A*) Two copies of the cytosolic N-terminal segment of TRPML1 (underlined with black color) were fused with either GFP or mCherry. Amino acid residues (R^{42-44}, K^{55}, R^{57}, R^{61}, K^{62}; in magenta) were mutated in the ML1N-7Q*2 construct; R^{61} and K^{62} were mutated in the ML1N-2A*2 construct (magenta bold). The blue columns denote α-helices predicted by the PSIPRED software. (*B*) Cartoon illustration of the ML1N*2 probe (tandem repeat of an N-terminal segment of TRPML1, amino acid residues 1–68). Marked are the putative positively charged phosphoinositide-interacting amino acid residues.

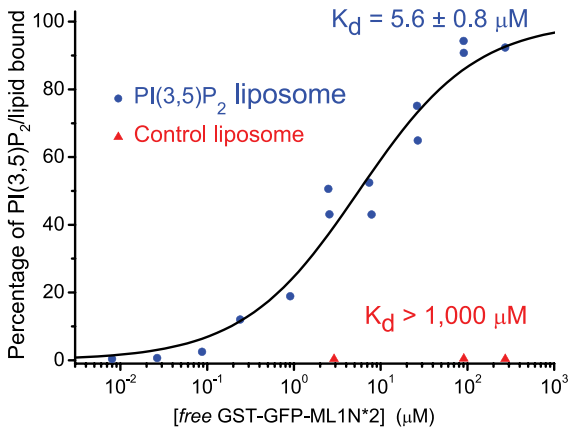

Fig. S2. Purified GST-GFP-ML1N*2 proteins bound to PI(3,5)P_2-containing liposomes. Purified GST-GFP-ML1N*2 proteins bound to PI(3,5)P_2-containing liposomes [65% phosphatidylcholine (PC), 30% phosphatidylethanolamine (PE), and 5% PI(3,5)P_2] with a K_d of 5.6 μM. No significant binding was observed for control liposomes with 70% PC and 30% PE.

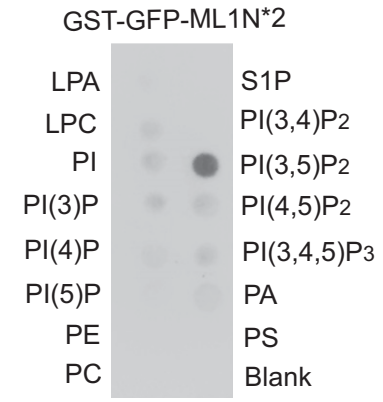

Fig. S3. GST-GFP-ML1N*2 selectively binds to PI(3,5)P_2 in a lipid strip assay. Protein–lipid overlay. The strip contained 15 different types of lipids including all 7 phosphoinositides. The purified GST-GFP-ML1N*2 proteins were used to probe the strip. Proteins bound to the strip were detected using anti-GST antibodies. LPA, lysophosphatidic acid; LPC, lysophosphocholine; PA, phosphatidic acid; PC, phosphatidylcholine; PE, phosphatidylethanolamine; PI, phosphatidylinositol; PS, phosphatidylserine; S1P, sphingosine-1-phosphate.

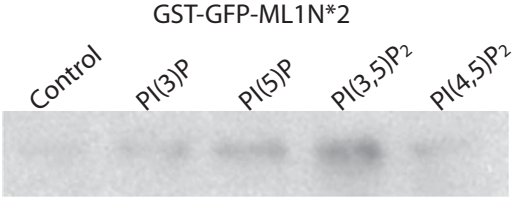

Fig. S4. GST-GFP-ML1N*2 selectively binds to PI(3,5)P_2 in a beads-binding assay. Purified GST-GFP-ML1N*2 proteins exhibited strong binding to PI(3,5)P_2-conjugated agarose beads, but weak or no binding to beads conjugated with PI(3)P, PI(5)P, or PI(4,5)P_2. Beads were diluted to a final concentration of 500 nM respective phosphoinositide and incubated with purified GST-GFP-ML1N*2 protein for 2 h. Proteins bound to beads were washed thoroughly and visualized by Western blot with anti-GST antibodies.

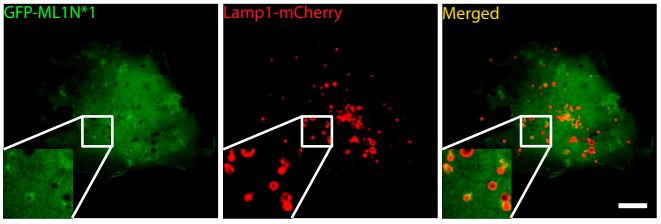

Fig. S5. The ML1N*1 probe is localized to the cytosol and a subset of Lamp1-positive compartments. COS1 cells were cotransfected with GFP-ML1N*1 and Lamp1-mCherry. (Scale bar: 10 μm.)

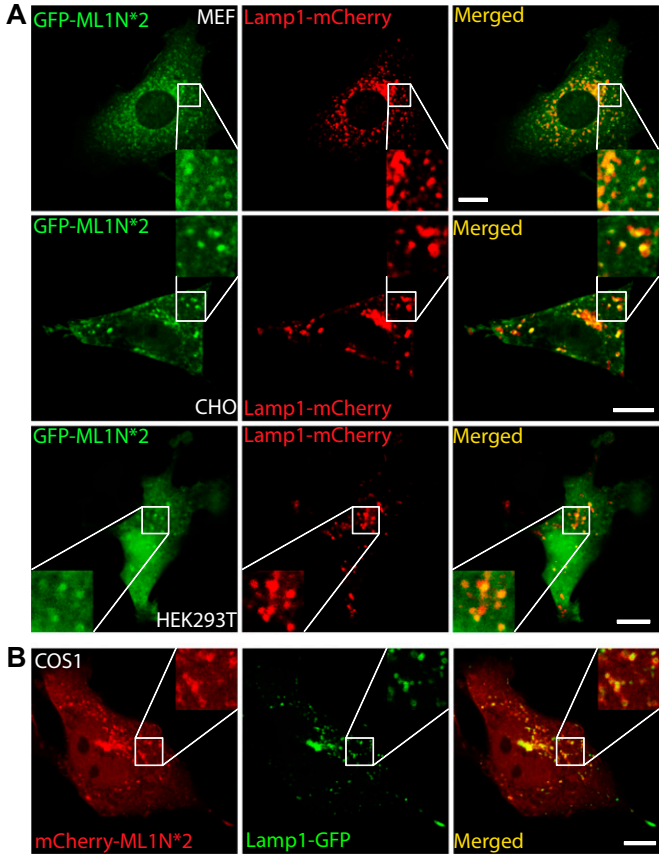

Fig. S6. Vacuolar localization of the ML1N*2 probe is independent of cell type and fluorescent tag. (*A*) Significant colocalizations between GFP-ML1N*2 and Lamp1-mCherry were observed in various cell types, including MEF (top panels), CHO (middle panels), and HEK293T (bottom panels). (*B*) Colocalization between ML1N*2 and Lamp1 in COS1 cells that were cotransfected with mCherry-ML1N*2 and Lamp1-GFP. (Scale bar: 10 μm.)

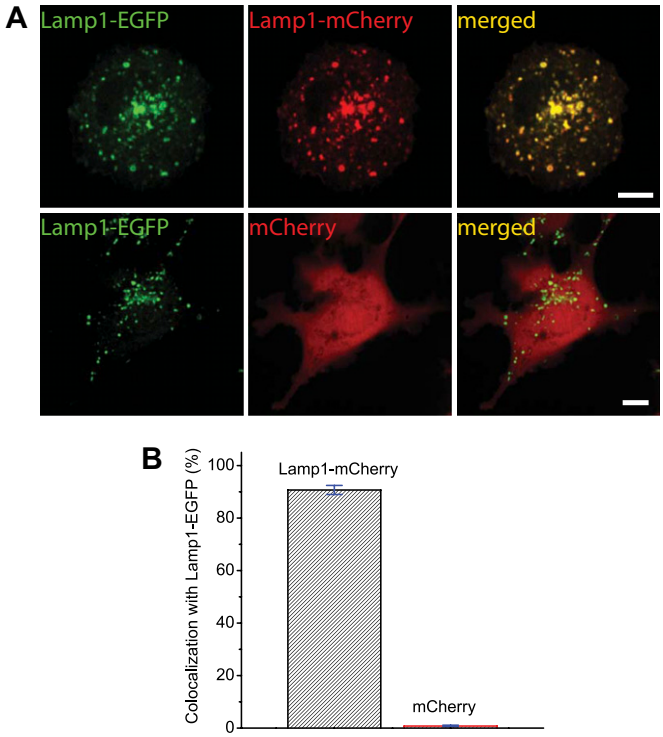

Fig. S7. The colocalization index reflects well the degree of colocalization. (*A*) COS1 cells were cotransfected with either Lamp1-mCherry + Lamp1-EGFP, or mCherry + Lamp1-EGFP. Note that although Lamp1-EGFP fluorescence was spatially colocalized with the mCherry fluorescence (appeared yellow in the merged image), with the colocalization algorithm used (*SI Materials and Methods*) they should show minimal colocalization because the mCherry fluorescence is not above 50% of its cytosolic background. (*B*) Statistical analysis of colocalization index ($n = 10$ for Lamp1-EGFP vs. Lamp1-mCherry, and $n = 13$ for Lamp1-EGFP vs. mCherry). (Scale bars: 10 μm.)

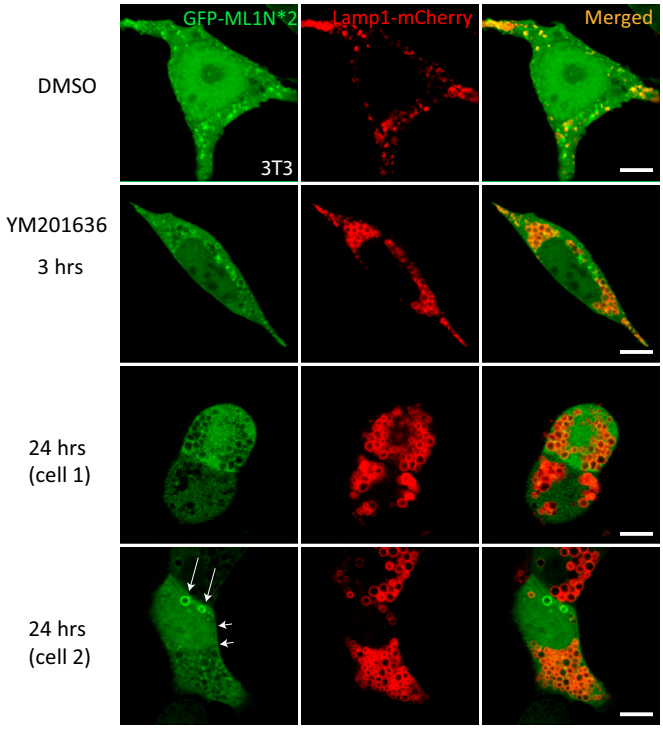

Fig. S8. Lysosomal localization of the GFP-ML1N*2 probe is sensitive to YM201636 treatment in NIH 3T3 cells. NIH 3T3 cells were cotransfected with GFP-ML1N*2 and Lamp1-mCherry plasmids. Cells were treated with 1.6 μM YM201636 for the indicated lengths of time or DMSO for 3 or 24 h. GFP-ML1N*2 dissociated from Lamp2-mCherry–positive compartments after YM201636 treatment. In a subset of cells, patchy plasma membrane (PM) localization (arrowheads) and few GFP-positive vesicles (arrows) were still observed after 24 h of YM201636 treatment. (Scale bar: 10 μm.)

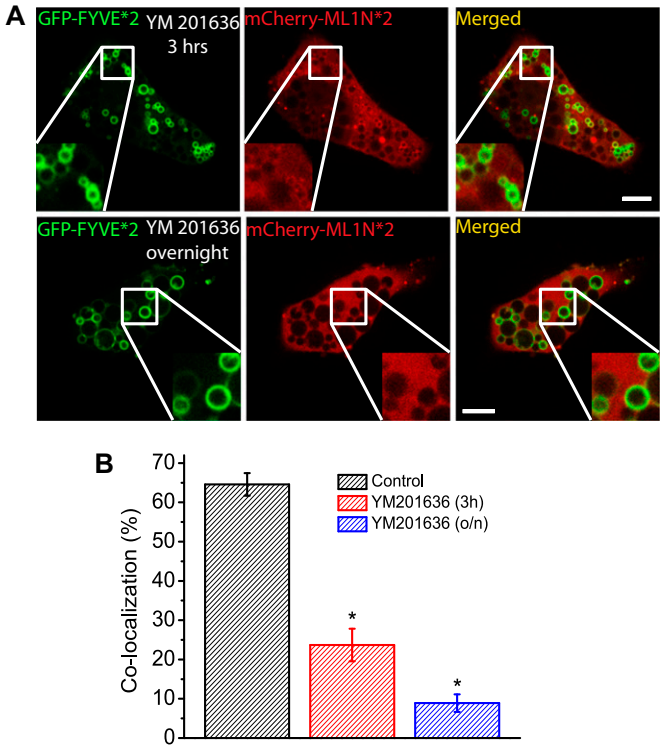

Fig. S9. Inhibition of PI(3,5)P_2 synthesis reduces the colocalization between the PI(3)P and PI(3,5)P_2 probes. (*A*) COS1 cells were cotransfected with the PI(3)P probe GFP-Hrs-FYVE*2 and mCherry-ML1N*2, and were then treated with YM201636 for 3 h (*Upper*) or overnight (*Lower*). (*B*) The colocalization index between GFP-Hrs-FYVE*2 and mCherry-ML1N*2 was reduced by YM201636 treatment for 3 h (23.7 ± 4.2%, $n = 12$) or overnight (8.9 ± 2.2%, $n = 12$), compared with nontreated cells (64.6 ± 2.9%, $n = 30$). Error bars represent SEM. The asterisk indicates $P < 10^{-5}$. (Scale bar: 10 μm.)

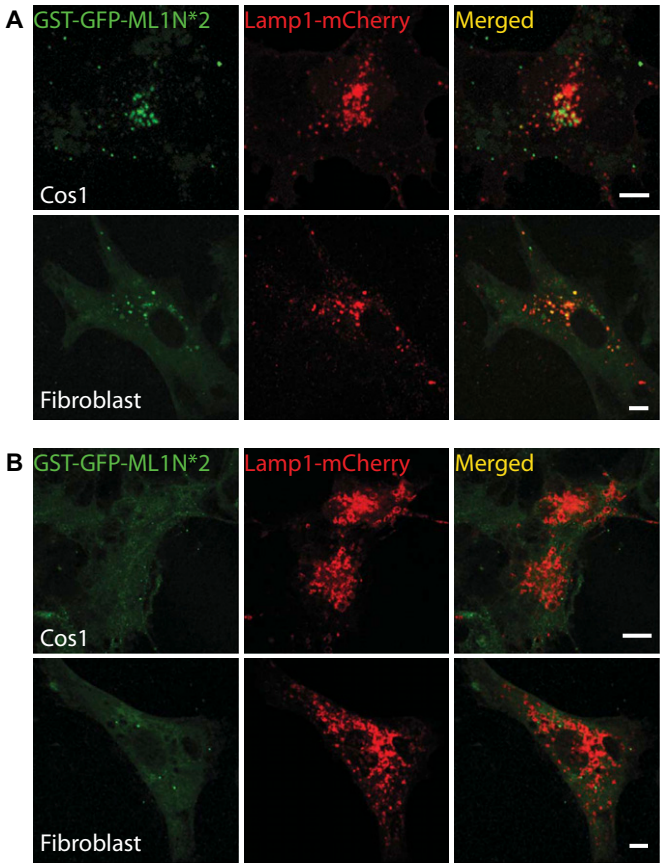

Fig. S10. Detection of endogenous PI(3,5)P_2 in living cells using exogenously applied purified GST-GFP-ML1N*2 proteins. (*A* and *B*) Lamp1-mCherry–transfected COS1 cells or fibroblasts were treated without (*A*) or with (*B*) 1 μM YM 201636 for 30 min, fixed, blocked, and then incubated with exogenously applied purified GST-GFP-ML1N*2 protein (*SI Materials and Methods*). GFP fluorescence showed clear colocalization with Lamp1-mCherry in *A*. Cells treated with YM 201636 exhibited mostly diffuse or background fluorescence. (Scale bar: 10 μm.)

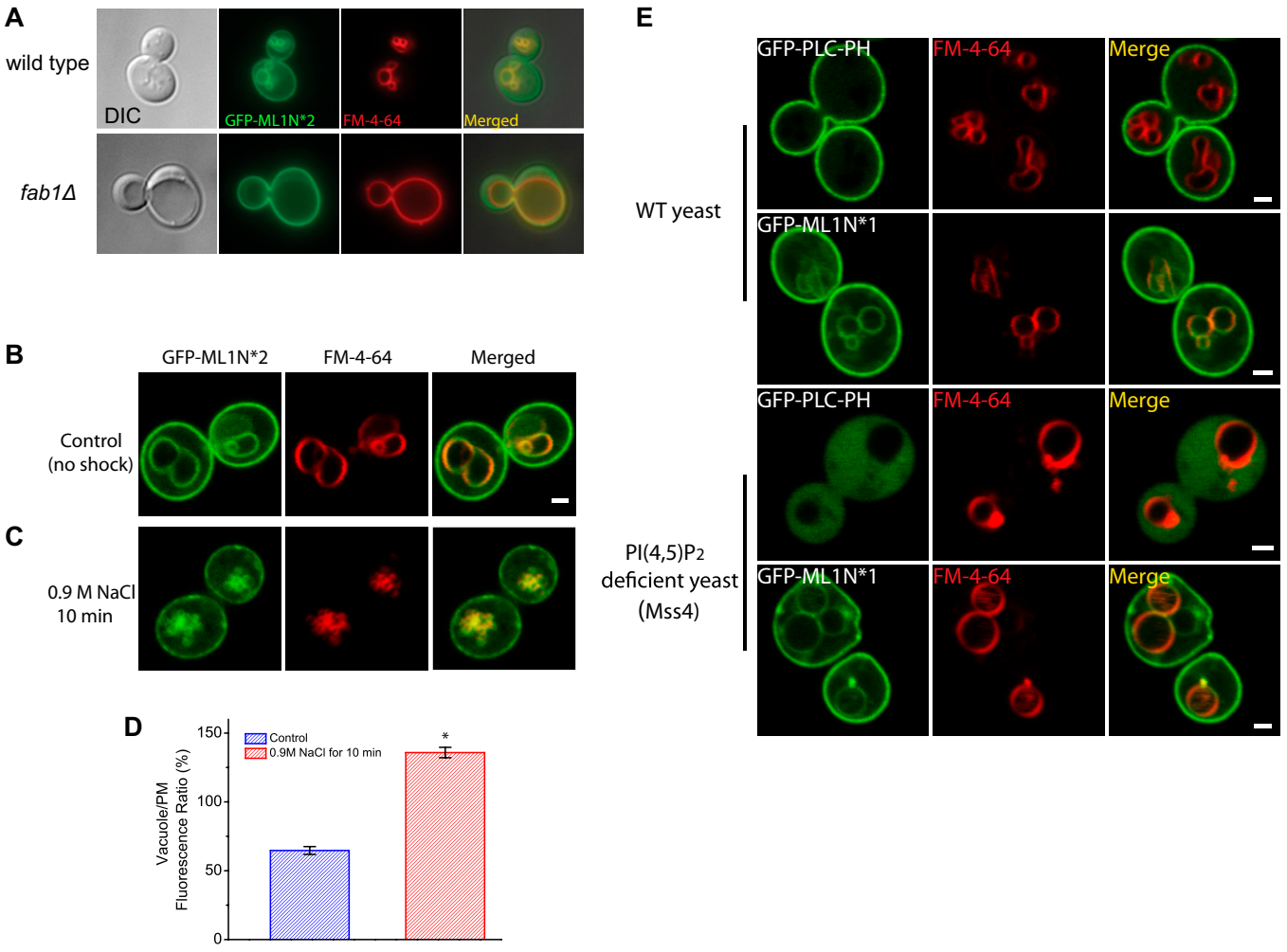

Fig. S11. Detection of PI(3,5)P_2 on yeast vacuoles by the probe. (*A*) Vacuoles were labeled with the FM4-64 dye in WT (upper panels) and *fab1Δ* (lower panels) yeast cells transformed with a plasmid expressing GFP-ML1N*2 from an ADH promoter. (Scale bar: 5 μm.) (*B*) Increased enrichment of the PI(3,5)P_2 probe on the vacuolar membranes by hypertonic shock in yeast cells. WT yeast cells were transformed with a plasmid expressing GFP-ML1N*2 from an ADH promoter and stained with FM-4-64 to visualize the vacuole membranes. (*C*) The response of WT yeast cells upon hypertonic shock by addition of 0.9 M NaCl. (*D*) Hypertonic shock decreases the ratio of fluorescent intensity on plasma membrane (PM) versus vacuole membrane. A total of 36 (for control) and 25 (for hypertonic shock) yeast cells from three independent experiments were analyzed. The asterisk indicates $P < 10^{-5}$. (Scale bars: 1 μm.) (*E*) The plasma membrane localization of GFP-ML1N*1 in yeast cells is not due to PI(4,5)P_2. (*Upper*) The localization of PI(4,5)P_2 probe (GFP-PLCδ-PH) and GFP-ML1N*1 in WT yeast cells. PI(4,5)P_2 probe was localized exclusively to the plasma membrane, whereas GFP-ML1N*1 was localized to both plasma membrane and vacuole membranes. (*Lower*) The localization of GFP-PLCδ-PH and GFP-ML1N*1 in PI(4,5)P_2-deficient Mss4 mutant yeast cells (1). (Scale bars: 1 μm.)

1. Desrivières S, Cooke FT, Parker PJ, Hall MN (1998) MSS4, a phosphatidylinositol-4-phosphate 5-kinase required for organization of the actin cytoskeleton in *Saccharomyces cerevisiae*. *J Biol Chem* 273(25):15787–15793.

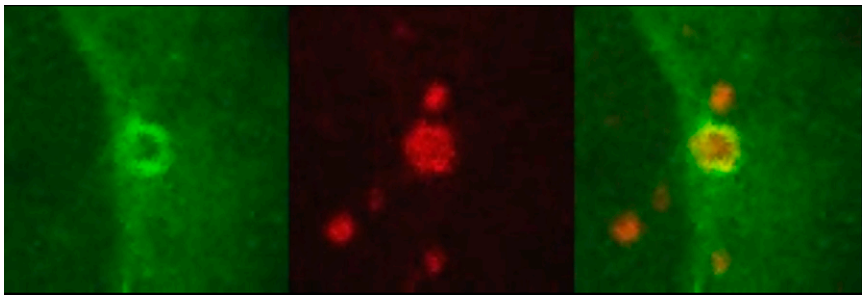

Movie S1. Changes in the probe intensity on the vacuolar membranes in GFP-ML1N*2 and Lamp1-mCherry dually transfected COS1 cells (for the experimental conditions and images, see Fig. 4*C* and figure legends).

Movie S1

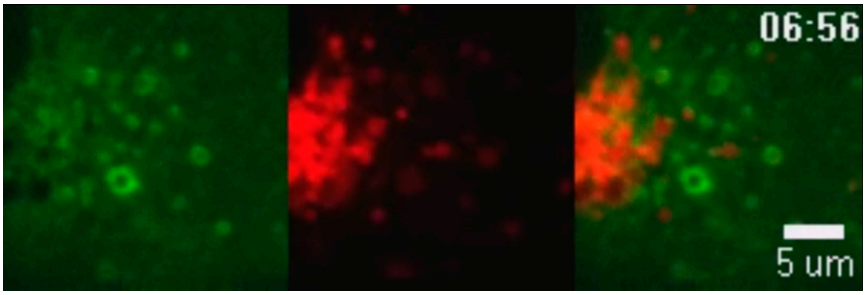

Movie S2. Time-lapse imaging of the fusion events in GFP-ML1N*2 and Lamp1-mCherry dually transfected COS1 cells (for the experimental conditions and images, see Fig. 4*D* and figure legends).

Movie S2

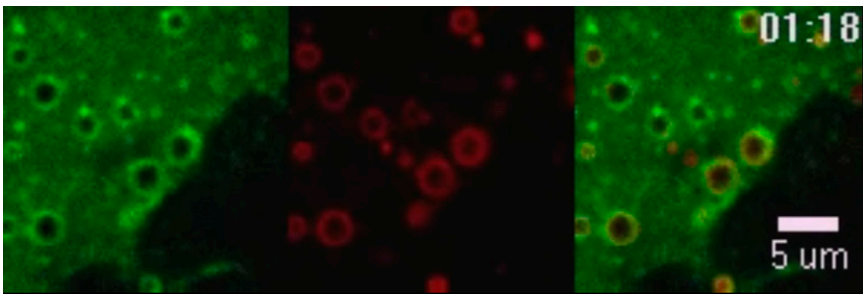

Movie S3. Time-lapse imaging of the fusion events in GFP-ML1N*2 and Lamp1-mCherry dually transfected COS1 cells (for the experimental conditions and images, see Fig. 4*E* and figure legends).

Movie S3